Oxygen driven reconstruction dynamics of Ni(977) measured by time-lapse scanning tunneling microscopy

T. P. Pearl[a] and S. J. Sibener[b]
The James Franck Institute and the Department of Chemistry, The University of Chicago, Chicago, Illinois 60637

(Received 13 March 2001; accepted 7 May 2001)

Time-lapse scanning tunneling microscopy (STM) has been used to observe the oxygen induced reconstruction behavior of Ni(977), a stepped metallic surface. Previous studies using helium atom diffraction resolved the macroscopic kinetics for the reversible step-doubling and -singling of this vicinal surface. Sequential STM imaging recorded at elevated temperature has now elucidated atomic-level mechanistic details for the merging of steps in the presence of small amounts of adsorbed oxygen, less than 2% of a monolayer. Point contact between neighboring steps decorated with chemisorbed oxygen facilitates rapid step coalescence by means of zippering. An optimal oxygen concentration of step edge saturation was found to enable the step merging to proceed most rapidly. Excess oxygen was found to hinder the coalescence of neighboring steps through the possible growth of overlayer structures on the terraces. At sufficiently high temperatures, the surface is driven back to single steps due to oxygen dissolution. The departure of oxygen from the surface through dissolution, as well as the associated presence of oxygen in the selvedge region, may both play a role in destabilizing the double steps. Local step density influences the coalescence behavior by defining the number of available step edge sites. The microscopic details made available by time-resolved STM imaging illuminate some of the mechanistic steps related to the initial stages of metallic oxidation, and the sensitivity of surface morphological transformations to local surface structure and adsorbate coverage. © *2001 American Institute of Physics.*
[DOI: 10.1063/1.1381532]

I. INTRODUCTION

Surface morphology and local structure play a large role in determining surface reaction rates and pathways. Defects like steps, kinks, and those having more complex local geometries influence interface energetics that determine the mechanisms for surface passivation, catalysis, nucleation, corrosion, and overlayer structure transitions. Deviations in surface electronic and phonon structure from the flat terraces directly affect the interactions of an adsorbed atom or molecule with the surface. One way of probing the behavior of departures from perfect crystal planes is to introduce a periodic defect array like that found on a vicinal, i.e., stepped, surface. Carefully prepared vicinal systems exhibit a predictable crystallographic orientation and therefore a controlled step density and geometry. The chemical reactivity, physical and metallurgical properties of imperfect surfaces can be further understood and the role of features like steps in influencing surface reactions can be quantified with these samples. In order to better comprehend the role of defects in metallic oxidation as well as other surface reaction mechanisms we have chosen to study the Ni(977) system using both local probe and scattering techniques.

Stepped surfaces have been observed to undergo a wide variety of surface reconstructions and structural phase transitions.[1–30] The delicate thermodynamic balance that determines equilibrium crystal shape governs the degree of orientational instability.[31,32] Changes range from irreversible faceting of the surface, i.e., alteration of crystallographic geometry, to more subtle modifications of step–step interaction energetics. The extent to which different surfaces reconstruct has been shown to be a function of both the material and vicinal miscut. Vicinals of (100) and (110) planes tend to exhibit more radical transformations with and without the presence of adsorbates due to the higher levels of corrugation compared to the close packed (111) miscuts. Terrace reconstructions or interlayer and row relaxations can further complicate stepped surface topography. Binding energies for adsorbates, which contribute to the overall surface free energy balance, will depend on the surface orientation and the material involved. There is a class of adsorbate mediated modifications in step–step interactions that cause stepped metal surfaces in particular to be driven from their clean surface step arrangement. The morphological transformations of various stepped metal systems have been studied recently using both local probe imaging and reciprocal space scattering techniques including Pt,[1–5,14] Ni,[6–9,24,30] Rh,[10,11] Cu,[12,13,16–21] Mo,[15] W,[22,23] Ag,[25,26] and Au.[27] Different adsorbates and impurity levels have been studied, including C, S, and O, which have been observed to influence the step energetics and the balance of surface free energy. The sensitivity of stepped metal surfaces to adsorbate coverage, temperature

[a]Present address: Department of Chemistry, The Pennsylvania State University, 152 Davey Laboratory, University Park, Pennsylvania 16802.
[b]Author to whom correspondence should be addressed. Electronic mail: s-sibener@uchicago.edu

and sample preparation has been well established. Further descriptions of the surface thermodynamics will be presented later in this section.

Various experimental and theoretical approaches have been undertaken to uncover the rich morphological behavior of stepped metal surfaces. Scattering techniques including low energy electron diffraction (LEED) and helium atom scattering (HAS) have been used to track shifts in long range order arising from structural phase transitions.[1,4–6,10,11,22–24,30] Reciprocal space diffraction rods, however, are limited to reflecting only the average behavior over the region sampled. Information lost in the long-range statistics is paramount to a fundamental understanding of how many surface processes progress, including stepped surface reconstructions. In order to elucidate some of the local details of stepped surface transformations, we have chosen to investigate the behavior of Ni(977) using scanning tunneling microscopy (STM). Time-lapse imaging of surface reconstructions on this vicinal system has been performed and the results have provided great insights into the nature of step–step interactions and surface mass transport mechanisms.

A. Influences on step energetics

The equilibrium step array configuration for a vicinal system is determined by the minimization of surface free energy derived from summing the energies associated with the terraces, isolated steps, and step–step interactions.[31] The free energy density, $f(T)$, for a surface of vicinal miscut ϕ, can be expressed as

$$f(T)=\gamma_0(T)+(\beta_0-TS(T))\cdot\frac{|\tan\phi|}{h}+Tg(T)\left(\frac{|\tan\phi|}{h}\right)^3$$
$$=\gamma_0(T)+\beta\left(\frac{|\tan\phi|}{h}\right)+g|\tan\phi|^3, \quad (1)$$

where γ_0 is the free energy of the terraces, β is the free energy per unit step edge length for forming an isolated single layer height step, and g represents step–step interactions. Free energy for step formation is a function of kink excitations that lead to step wandering through an increase in entropy.

The energetic and entropic terms that determine step–step interactions, and consequently equilibrium surface structure, arise from a variety of properties associated with both individual steps and the entire ensemble of steps. Distribution of charge across a step edge boundary sets up a primarily vertically aligned dipole (Smoluchowski effect[33]) and this introduces a repulsive electrostatic interaction between step edges.[14,34] The other issue is the entropy associated with step meandering. The entropy for step wandering is largest in the limit of lowest step density. As step edges are brought closer together, the entropy for wandering decreases causing an entropic repulsion between the steps based on a no-crossing condition for adjacent edges.[31,35] Introduction of adsorbates, especially strongly bound ones like C, S, and O, however can significantly influence the nature of these repulsions. Many low temperature STM studies of adsorbate interactions on both stepped surfaces and nominally flat surfaces with isolated steps have shown how substrate and adsorbate properties communicate particularly in the nature of surface electronic structure perturbation.[36–39] Dipoles at the step edges are susceptible to modification by the presence of adsorbates. Entropy associated with step wandering can increase if coalescence becomes more favorable by a reduction in the repulsive electrostatic interaction between step edge dipoles. The energy associated with step edge mobility and kink formation can be influenced by adsorbates bound to step edges. Additionally, in the case of the doubling on the Ni(977) surface and other vicinals, adsorbates like oxygen are thought to change the thermodynamic balance in favor of merged step edges. Depending on the crystallographic orientation of the step face, there can exist a driving force for merging if the oxygen prefers the binding sites available at the step edges. All of these factors operate in concert to mediate a change in equilibrium morphology. For the oxygen driven surface reconstruction on Ni(977) the oxygen plays the role in introducing a decrease in terrace free energy and an increase in step edge free energy along with a modification to the step–step interaction.

B. Previous studies on Ni(977) surface properties

The surface structural phase transitions, step-localized phonon modes, energy exchange in inelastic multiphonon scattering, overlayer stabilization, and templating effects of the Ni(977) surface have been studied extensively in our group using helium atom scattering and low energy electron diffraction.[30,40–43] Theoretical modeling has also been performed recently on this surface with respect to its step doubling and phonon structure.[44–46] The reconstruction kinetics of the Ni(977) surface transformations were mapped out using helium diffraction.[30] Experiments were performed by either monitoring the change in terrace width or step height as a function of time using judicious scattering kinematics and crystal orientation. It was shown that the surface structure could be driven from its nascent single step phase to a double step arrangement (Fig. 1) with a small exposure of oxygen (<0.2 Langmuirs) over the temperature range of 390–470 K. This transformation was found to be reversible with changes in surface temperature or oxygen concentration. Figure 2 is a reaction sequence diagram that illustrates the step phases between which the surface can be driven. These reconstructions precede bulk oxidation and irreversible faceting of the surface and occur over a temperature range that is bound on the lower end by the thermally activated diffusion of Ni and on the upper end by the temperature at which step edge adsorbed oxygen dissolves into the bulk. As a function of temperature for a single coverage of oxygen, the surface was found to undergo the doubling transition with second order kinetics with respect to the single step density. At temperatures above the doubling range, the system would revert to its single step phase with first order kinetics with respect to the double step density. The first order resingling was assumed to be due to a dissolution process that would destabilize the merged steps.

The helium scattering data, though limited to long-range order, provided some insight into the microscopic details for doubling by elucidating the doubling rate dependence on sur-

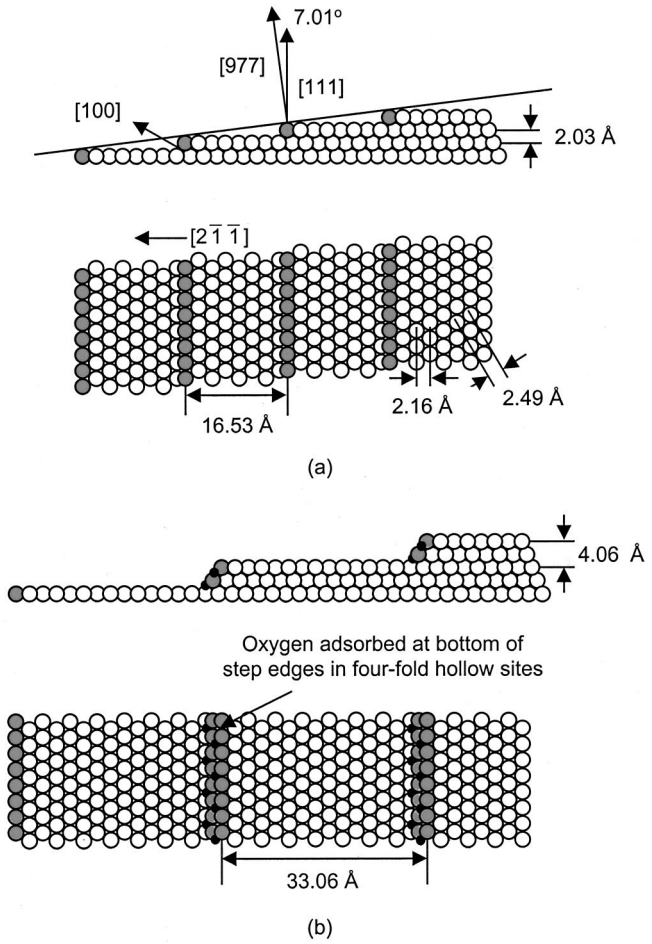

FIG. 1. A schematic illustration of the (a) single step and (b) double step configurations for Ni(977). Several crystallographic dimensions and high symmetry directions are indicated. The clean, single step structure for this surface is composed of (111) terraces, 8 atomic rows wide, separated by monatomic (100) risers. For the doubled surface, the (111) terraces extend to 15 atomic rows and the height is doubled. The oxygen that mediates the structural transition is believed to be adsorbed preferentially at the bottom of the steps.

face temperature and oxygen coverage. The diffraction observation indicates that oxygen adsorbed at the (100) step edges provides the thermodynamic driving force for the coalescence of single steps into doubles. Oxygen has been found to preferentially adsorb at four fold coordinates sites like those available at (100) step faces (Fig. 1).[9,13,47] Optimal coverage for doubling at a given temperature corresponded roughly to the number of step edge sites available on the single stepped surface. The kinetics data illuminated some of the possibilities regarding the mechanism and the rate limiting steps for the doubling. From an Arrhenius analysis of the temperature dependence on the doubling rate an activation energy was extracted that agreed with the approximate energy necessary for breaking a single bond in a metal. This implies that the activation energy is associated with the detachment of a single Ni atom or O–Ni complex from a step edge kink site. The oxygen concentrations involved suggest that its diffusion would not be rate limiting. Some of these issues regarding the role of the oxygen and the temperature in the mechanism for doubling can now be addressed using local probe microscopy.

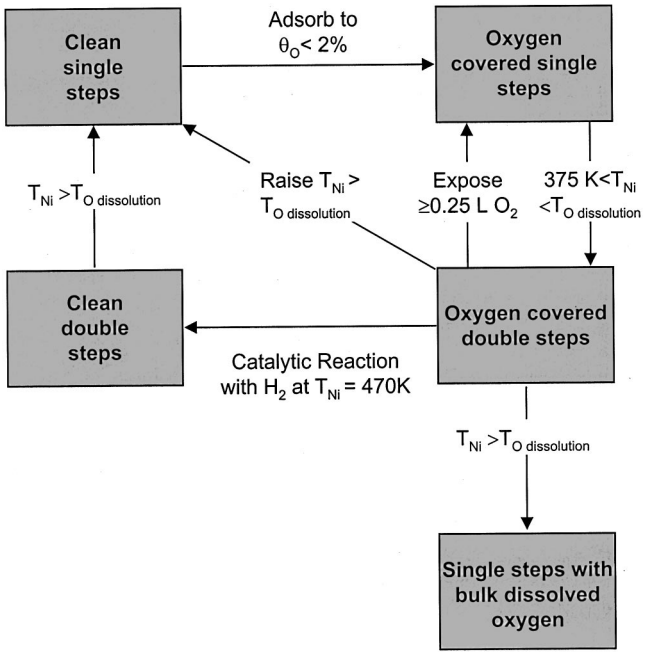

FIG. 2. Reaction sequence diagram illustrating the different oxygen and heat driven structural transformations that occur for Ni(977). This particular STM study focused on the doubling and resingling behavior of the surface as a function of oxygen exposure.

Modeling of the step-doubling transition on Ni(977) and Rh(332) was performed by Khare *et al.*[44] Using Monte Carlo methods, the step-doubling dynamics was considered on these surfaces using a terrace-step-kink (TSK) model where step meandering is the only thermal excitation. The upshot of the theoretical study was that steps would rapidly merge once contact was made and that the diffusion of one step to another by meandering was the limiting step. The calculations did not, however, account for the role of oxygen in enabling or mediating the merging of steps.

The step dynamics of Ni(977) have now being studied using STM. We designed and constructed a variable temperature UHV-STM system to study step behavior and surface reactivity.[48] While the HAS data has provided statistical information about the changes in long range order with the macroscopic kinetics, with STM we are capable of creating real-time movies of the surface reconstruction on a local scale. There have been various studies aimed at correlating reciprocal and real space data in order to arrive at a more complete description of surface phenomena. STM has been paired with neutral atom scattering, electron diffraction, and other surface sensitive techniques in order to arrive at more complete descriptions of surface phenomena.[2,3,7,8,13–15,19] The time scale for the reconstruction on Ni(977) has allowed us to use the STM to resolve the merging of the steps at temperature in real time. We have been able to exploit the relatively slow kinetics of the transformation on this surface and generate the first real-time capture of this class of surface reconstruction using a local probe technique. The real space local information procured from time-resolved STM images ideally complements the extensive macroscopic kinetics database produced by HAS. The STM is capable of routinely resolving monatomic and multiatom high steps on metals at

elevated temperatures and is an ideal tool for capturing surface dynamics that occur on such long time scales.

II. EXPERIMENT

A. Instrumentation

The STM experiments were performed in a two-stage stainless steel UHV chamber with a base pressure of 5.5×10^{-11} Torr. The experimental system is supported on a steel frame that is bolted to pneumatic vibration isolators. Chamber pumping is achieved by a 220 l/s D–I ion pump, cryoshroud and titanium sublimation pump as well as a 55 l/s turbomolecular drag pump used for pumping sputtering gases and chamber bakeouts. During STM experiments, the turbomolecular drag pump is turned off along with its mechanical forepump to eliminate vibrational noise. The upper level of the chamber is equipped with standard tools for sample preparation and characterization. A retractable 4-grid low energy electron diffraction (LEED) optics is used for surface diffraction and surface cleanliness is checked by Auger electron spectroscopy (AES) by utilizing the optics as a retarding field analyzer (RFA). A sample stage with two docking stations, one for electron bombardment heating and the other for resistive heating, is mounted on an *XYZ* translator and polar drive. Single crystal metal samples are cleaned by ion sputtering cycles in combination with annealing by electron bombardment. A residual gas analyzer performs routine partial pressure analysis. Dosing of sputtering and reagent gases by chamber backfilling is done using high precision leak valves.

The lower level houses the STM and a load lock assembly for transferring samples in and out of vacuum. Transfer of samples between the sample preparation stage and the STM or the load lock magnetic linear drive are accomplished using a versatile pincer grip with $\pm 22.5°$ articulation tilt range, 360° rotation, and 8 in. of linear travel. The microscope used in the system is an Omicron Micro-STM supported by a Viton® elastomer stack attached to a flange. Microscope control electronics are from Topometrix (model ECU+) which consist of a low electronic noise feedback control and scalable voltage power supply for piezo motion in conjunction with an adapter unit that operates the coarse positioning of the STM scanner and the sample in the STM. All of the modalities of the Omicron STM have been maintained with the Topometrix driving electronics. Samples are held upside down in a molybdenum holder that rests on three piezo inertia motors for coarse positioning. The tip, cut from a 90% Pt/10% Ir wire, approaches the sample from below and is held with a set screw at the top of a four quadrant piezo electric ceramic tube attached to a coarse *Z* inertial motor which translates by a stick and slip mechanism. The single crystal metal samples, typically 0.500 in. in diameter and 0.100 in. thick used in our experiments are mounted on molybdenum platens with small molybdenum clips. A circular opening is machined in the platens for direct access to the rear of the sample for heating. Elevated temperature imaging of metal samples is made possible through the use of a radiative heater that can be positioned directly behind the sample. The details of the design of a proximity heater (Fig. 3) used for performing these experiments have been described in detail elsewhere.[48]

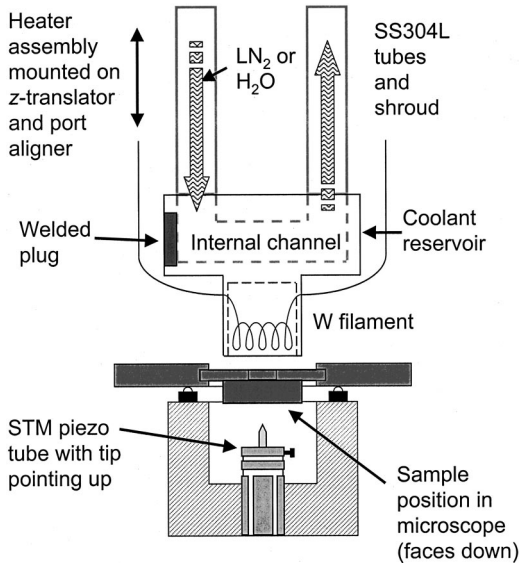

FIG. 3. Schematic drawing of the proximity heater used for performing STM experiments at elevated temperature and its relative position with respect to the STM. Use of a radiative heater suspended behind the sample allows for no additional mechanical coupling. The proximity heater assembly resides in a water or liquid cryogen cooled assembly to minimize radiative loading on nearby components; such cooling also mitigates vacuum contamination.

B. Sample preparation and experimental procedure

The Ni(977) surface was prepared by spark erosion cutting and mechanical polishing ($0.5\,\mu$m Al_2O_3) a Ni single crystal 7.01° away from the (111) face along the [21 1] direction. The crystal orientation was verified to within 0.5° of the (977) plane with Laue x-ray backscattering. The ideal (977) surface is a kinkless vicinal consisting of 8 atomic row (111) terraces and monatomic (100) step faces (Fig. 1). The crystal was cleaned and prepared using repeated cycles of 1 keV Ar^+ sputtering (between 300 and 1100 K) until C and S levels dropped below our Auger detection limit and annealing at 1100 K. Surface order was confirmed and characterized using LEED and STM. The quality of the spot splitting in the electron diffraction due to the steps was used as a barometer for surface cleanliness as well since small concentrations of surface contaminants can affect the ability of the stepped arrangement to achieve long-range step separation coherence.[4]

After performing a sputter and anneal cycle the sample was allowed to cool to approximately the temperature at which an experiment was to be performed in the STM. Prior to placement of the sample in the STM, the microscope was preheated to the experimental temperature with a dummy sample so that the operating components of the microscope reached thermal stability. The dummy sample was then removed and the real sample placed into the microscope with the heater returned to the power setting corresponding to the experimental temperature. More details regarding the procedures used for imaging at elevated temperature with our design are described elsewhere.[48] Images of the clean surface

were taken to ensure that the STM was stable and that a well ordered region of the sample would be imaged for the dynamics experiment. The sample was then dosed with the STM tip retracted slightly by decreasing the tunneling current a factor of 10 to slightly lessen the physical shadowing and field effects due to tunneling. Oxygen was delivered to the surface by chamber backfilling high purity O_2 using a high precision Varian leak valve located at a port close to the STM. For the relatively dilute oxygen doses used in this experiment, the local pressure at the STM was measured to determine the true exposure to the crystal. The conditions for inducing reconstructions of the crystal, including temperature and oxygen coverage, were established using LEED before attempting to perform STM experiments. Care was taken to ensure that the oxygen dosing at both the sample preparation and STM sample mounts were relatively equal. Oxygen doses were performed typically between 1×10^{-8} and 5×10^{-8} Torr with the tunneling junction intact that produced the same results as dosing between 1×10^{-9} and 5×10^{-9} Torr at the LEED; doses were performed at temperature. Eierdal *et al.* also reported a factor of 10 reduction in effective exposure of the dosed gas to the sample area underneath their STM tip.[49] This was confirmed qualitatively in our system during the coverage dependent experiments. Once the exposure was complete, the tunneling current was reset and time-lapse imaging commenced. Experiments were attempted with the tip completely retracted so as to avoid tip effects on dosing but the time lost in re-entering tunneling feedback was costly with regards to capturing the dynamics. All of the exposures listed for different experiments are the approximate effective exposures of oxygen to the surface region illuminated by the tip.

Two different time-lapse experiments were performed using different image sizes and pixel densities. For the purpose of resolving microscopic kinetics, a larger 2000 Å $\times$2000 Å area with 500×500 pixel density ($\sim$70 s/image) was used. Imaging a larger region was intended to track the average structural change of the surface as a function of time. A smaller imaging area (1000 Å$\times$1000 Å) with lower pixel density (300×300) was employed for taking measurements on individual merging events. With these imaging settings a balance was struck between having better time resolution ($\sim$20–40 s/image) and still being able to image events up to 1000 Å in length with step edge resolution. Faster scanning rates are possible and would allow for even finer time resolution but step edge clarity would be compromised. A given area would be imaged for up to 1 h, the time at which the reconstruction reaches its asymptotic limit as determined from both the electron and helium diffraction. Imaging was performed in constant current mode with 1 nA tunneling current and 100 mV positive sample bias with respect to the tip. Images were generated by rastering the tip across the step edges in order to facilitate analysis and acquisition (drift compensation). The sample was sputter cleaned and annealed before each STM experiment to ensure optimal local ordering of the steps and to also prevent any oxygen dissolution into the bulk that might alter the reconstruction dynamic range.[30] After performing a STM experiment, the crystal would be checked periodically with LEED to confirm that surface reconstruction was indeed occurring for the experimental conditions used.

III. RESULTS AND DISCUSSION

A. Step-doubling kinetics

Doubling sequences were recorded (2000 Å$\times$2000 Å area) at various temperatures with the same effective exposure for each run (0.15 L O_2). Figure 4 shows a region of single steps at 465 K that exhibit a narrow terrace width distribution and a sharp one-dimensional Fourier transform performed across the step edges. Regions of long-range coherence for single step heights and widths were selected for the purpose of measuring kinetic rates in order to mimic the experiments performed in reciprocal space. An effective exposure of 0.15 L at these temperatures corresponds to approximately step edge saturation of oxygen where every other step site is filled [Fig. 1(b)]. The transformation of the surface over a long range is readily apparent in real time STM imaging as shown in Fig. 5 where four frames from a doubling sequence are presented. From these imaging sequences, a variety of observations were readily made regarding the nature of the step merging. Zippering of two steps was found to proceed after contact of one step edge was made with its neighbor in the downstairs direction ([21 1]). Further details regarding step energetics and the speed of individual step merging events appear elsewhere.[50] After a sequence was collected, a FFT of each image would be compiled to extract the changes in relative populations of different sized terraces. Peaks corresponding to single and double or wider steps would be integrated and normalized and tracked as a function of time (from image to image). Figure 6 shows the tracking of a FFT peak for single steps. A plot of the normalized integrated area of each single step peak as a function of time for doubling experiments performed at different temperature is shown in Fig. 7. The fits through these data are derived from the kinetic order for doubling determined from helium scattering.[30] Careful examination of the observed scattering intensity corresponding to the double step population, $[D]$, yielded second order kinetics in the single step concentration, $[S]$. Assuming that all of the steps on the surface are only singles and doubles, the doubling rate can be expressed as

$$\frac{d[D]}{dt}=k_d[S]^2=k_d(1-[D])^2, \tag{2}$$

$$[D]=D_0\left(1-\frac{1}{k_dt+1}\right), \tag{3}$$

where k_d is the doubling rate constant and D_0 is the final double step population. The second order fits are in close agreement with the data indicating that the area sampled with the STM reflects the overall behavior of the crystal as seen by diffraction. Energetics for the process can be extracted from this kinetics data with Arrhenius analysis using the conventional formula

$$K=A_0\left(\frac{-E_a}{k_bT}\right), \tag{4}$$

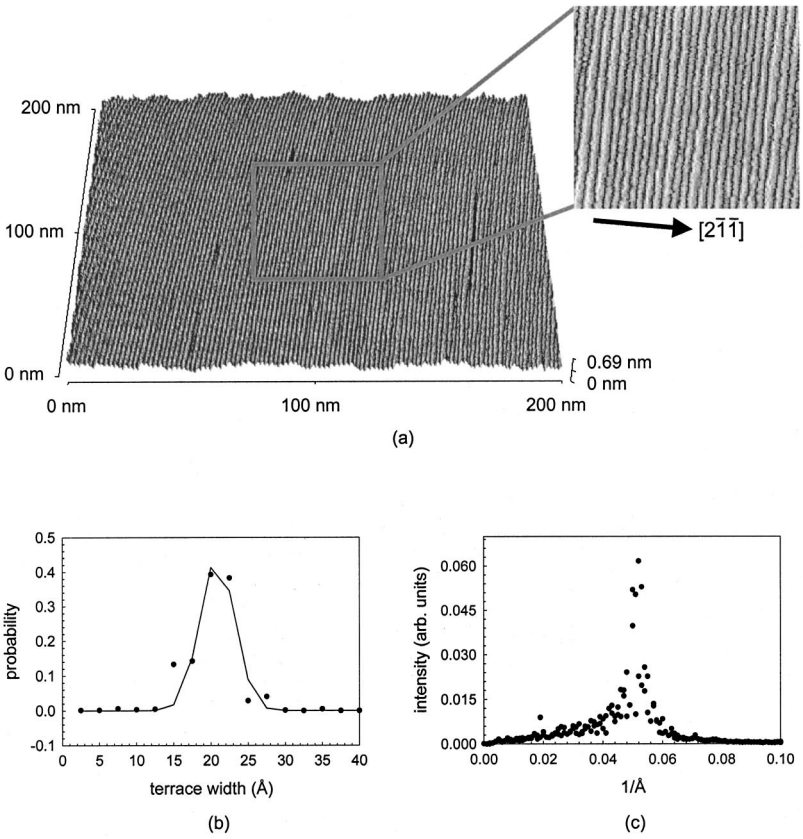

FIG. 4. (a) STM image (2000 Å×2000 Å area) of Ni(977) at 465 K taken with 100 mV sample bias and 1 nA tunneling current. A well-prepared surface will exhibit step width coherence for single steps over hundreds of angstroms. The downstairs direction for the step train is indicated in the zoomed in (500 Å ×500 Å) portion of the larger image. (b) and (c) The terrace width distribution and one-dimensional Fourier transform of the clean surface are indicators of the degree of ordering in the imaged region.

where E_a is the activation energy and A_0 is the preexponential factor. The results from the analysis are as follows: $E_a = 0.88 \pm 0.1$ eV and $A_0 = 10^{6.2 \pm 0.8}\,s^{-1}$ for 0.15 L effective O_2 exposure. The uncertainty in these measurements arises from a few factors. The temperature at which each experiment was performed had some drift due to the need for rapid exchange of samples at the STM. The second source of error comes in the FFT analysis where small changes in step resolution in individual images would exist, especially at elevated temperature, thereby affecting the relative backgrounds and peak intensities for the single step population contribution. Deviations from a smooth decrease in single step FFT signal do not correspond to real oscillations in the terrace widths. Measures were taken to correct for these variances by considering particularly noisy images with different background and normalization conditions. Analysis from the HAS experiments yielded $E_a = 0.52 \pm 0.03$ eV and $A_0 = 10^{3.1 \pm 0.3}\,s^{-1}$ for an oxygen coverage that roughly corresponds to step edge saturation. A range of activation energies between 0.4 and 0.9 eV was observed with HAS, attributed to sample history, specifically oxygen dissolution into the selvedge region. The values from the STM experiments are therefore in reasonable agreement with those extracted from the scattering data. Both results from the STM and HAS analyses for the activation energy fall into the range of predicted values for adatom migration energies on stepped Ni(111).[51]

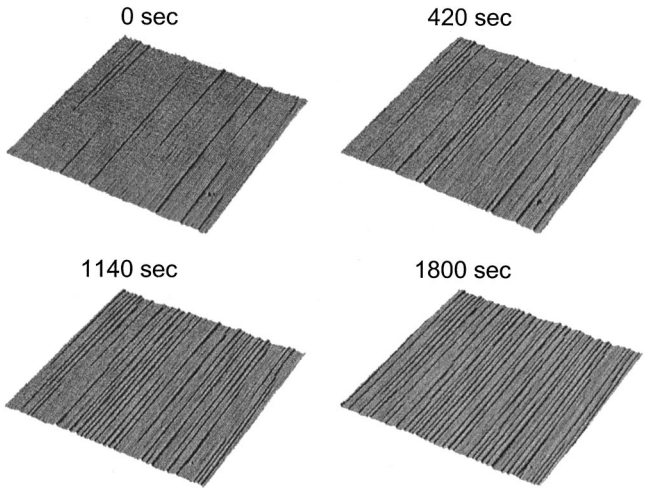

FIG. 5. Four frames from a doubling sequence where each image is 2000 Å×2000 Å in area and the imaging (100 mV sample bias, 1 nA tunneling current) was performed at 465 K after dosing the surface with 0.15 LO_2.

B. Coverage dependence on step-doubling rates

Doubling behavior was imaged (1000 Å×1000 Å) at one temperature (~465 K) and with various oxygen exposures. Regions of different step density or single step width population would be exposed to sequential doses of oxygen. For one type of experiment, a given region of steps would be exposed to a small amount of oxygen and then imaged. If after approximately 10 min no step merges had occurred, then more oxygen would be added and the region imaged again until there were no more discernible changes. This procedure would be repeated until the region reached its

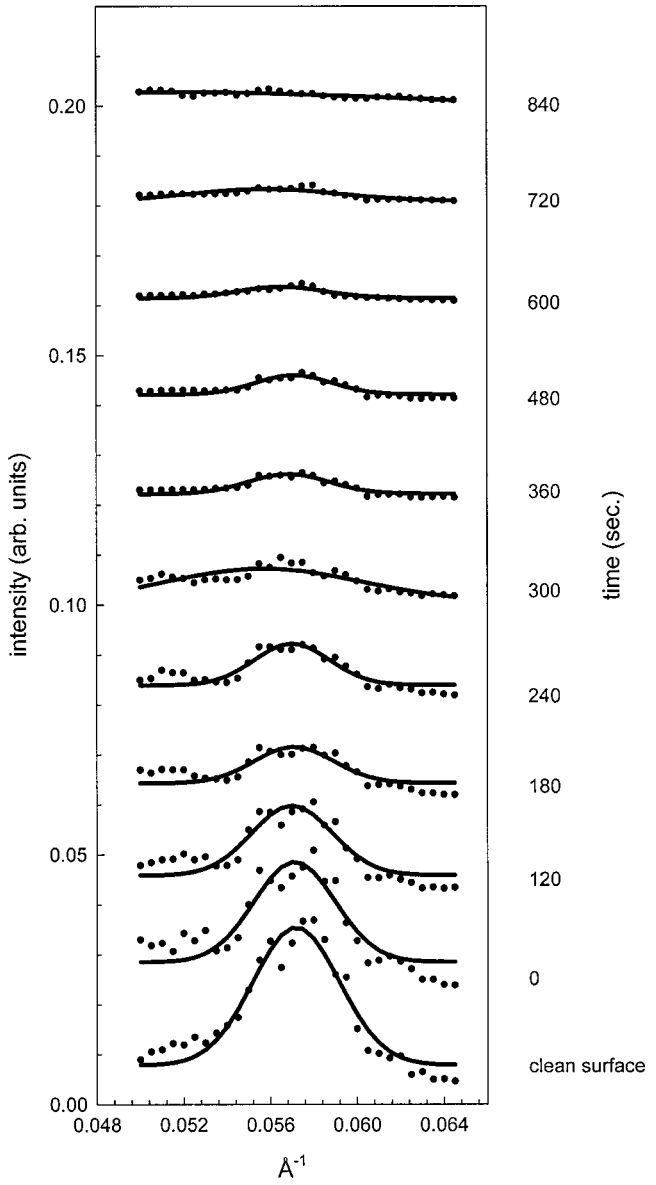

FIG. 6. FFT peak corresponding to single step widths as a function of time for $T_{xtal}=430$ K and 0.15 LO_2 exposure to the surface.

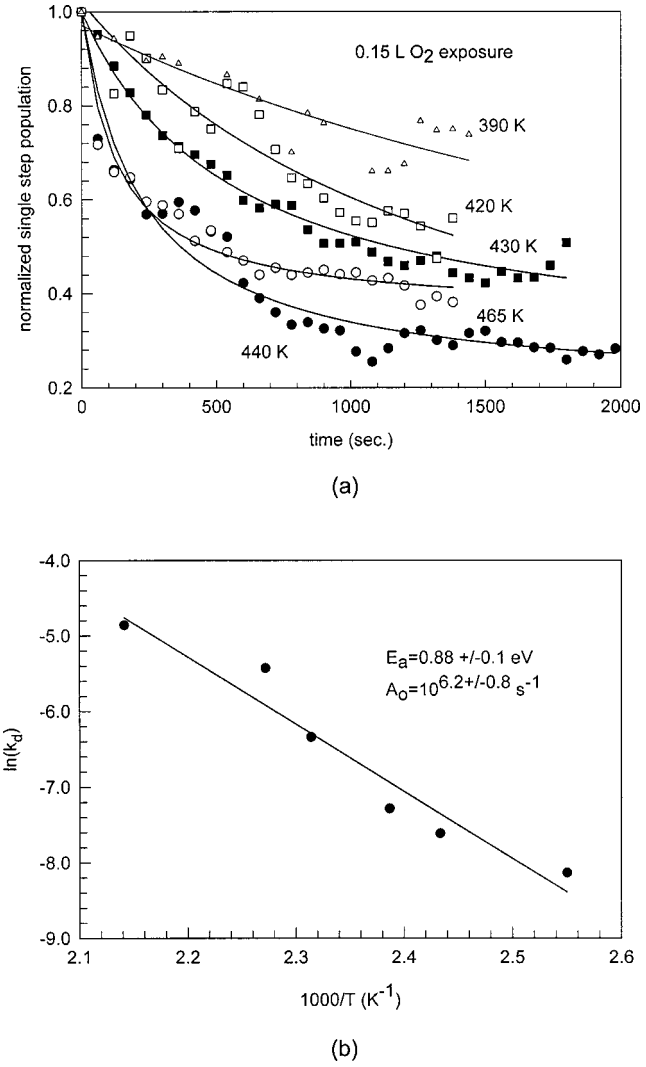

FIG. 7. (a) Doubling of the surface measured as a function of temperature for one oxygen exposure (0.15 L). Plotted is the drop in single step intensity as a function of time. (b) Arrhenius analysis performed on the temperature dependent data set reveals information regarding the energetics of this doubling transition. The activation energy and pre-exponential factor are in good agreement with previous experiments using helium atom scattering, low energy electron diffraction, and predicted values from theoretical studies for diffusion mechanisms on stepped nickel surfaces.

asymptotic limit for structural evolution. The entire sequence would then be analyzed by FFT to determine the surface response to the oxygen doses.

Plotted in Fig. 8(a) is an example of the evolution of doubling as a function of time and oxygen dose. The cumulative effective oxygen exposure for this run was 0.18 L which is roughly the amount of oxygen needed to cover all of the available step sites. The step array remains relatively stable with respect to reconstruction until the total amount of oxygen delivered to the surface reaches roughly step edge saturation at which point the surface begins to double rapidly. As a second example of the response of a well-ordered region to discrete doses of oxygen, Fig. 8(b) shows multiple kinks in the single and double step evolution curves corresponding to the various exposures. The differences in the overall exposure between the two examples can be attributed to deviations in uniform distribution of oxygen along the step edges (local aggregation). The other issue is the difference in the total number of steps in the imaging area. The first example [Fig. 8(a)] has an average terrace width of 17.3 Å compared to 21.7 Å for the second [Fig. 8(b)], which is approximately one extra terrace row. This variation translates into a difference of 12 steps between the areas and consequently fewer step sites available for the region that has slightly broader steps.

In the limit of small amounts of oxygen and long times, merging events are capable of occurring slowly. Sequences were recorded to assess the structural evolution for oxygen exposures much smaller than for step edge saturation. A minimum of 0.027 L O_2 exposure was found to produce any coalescence, which is approximately 1/6 of the exposure needed to achieve nominal step edge saturation. Figure 9 shows the last frame of a sequence along with the FFT tracking of single and double steps for a dose of 0.027 L O_2. Of particular note is the length of the merge events that occurred

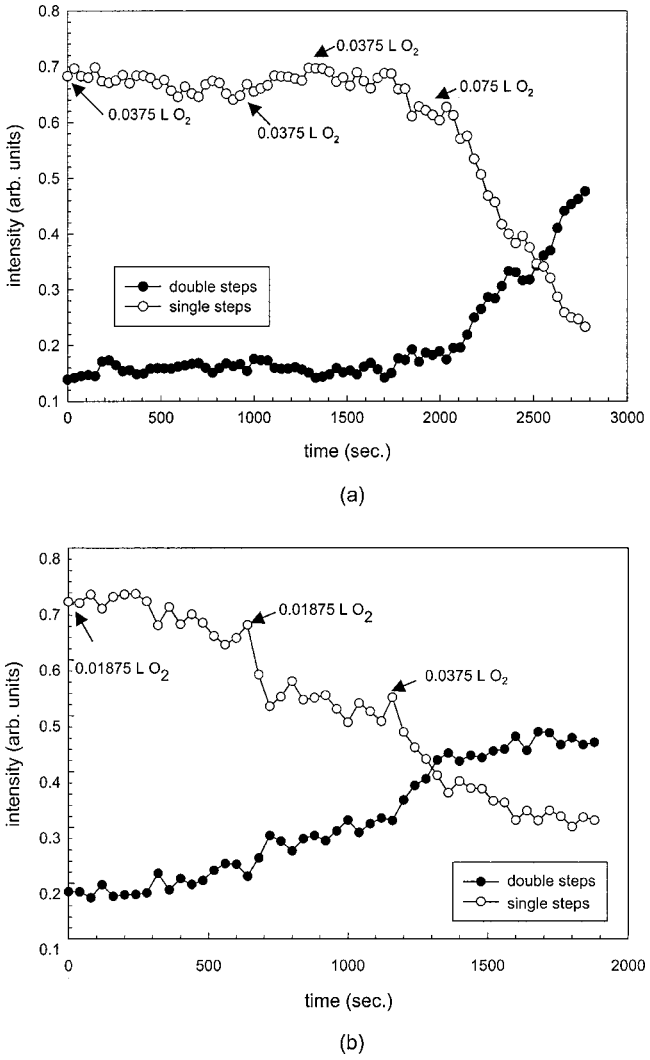

FIG. 8. Two different examples of the sensitivity of the doubling process to oxygen exposure at 465 K. Plotted are relative populations of single and double steps extracted from FFT peak intensities for two different regions from two different experiments that started as primarily single steps before being exposed to an initial dose of oxygen. Oxygen was exposed to the surface in discrete doses, as indicated in the plots with respect to timing and magnitude of dose, while the surface was undergoing reconstruction. In (a), the cumulative oxygen exposure was 0.1875 L and for (b) it was 0.075 L.

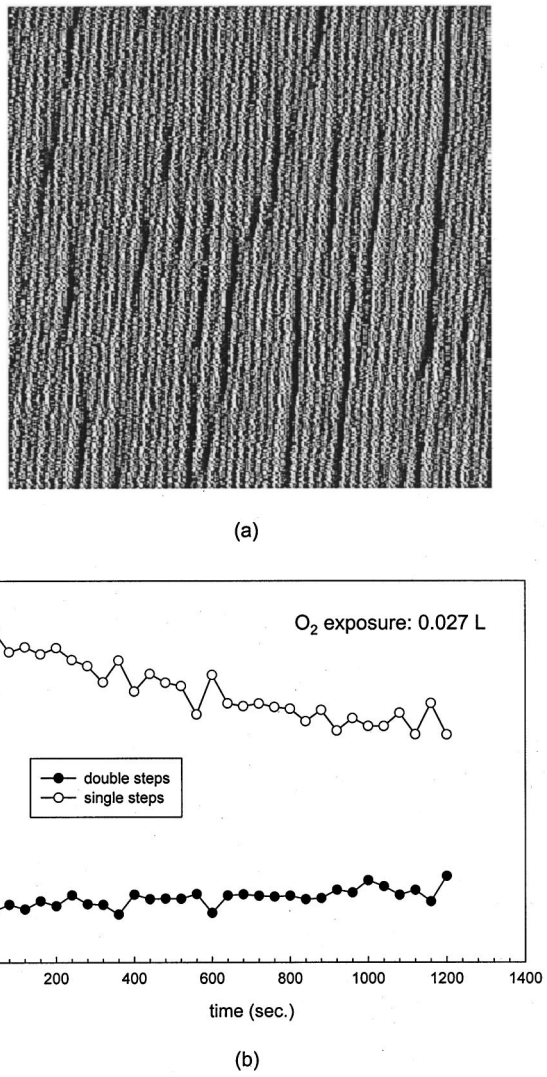

FIG. 9. (a) STM image ($1000\,\text{Å}\times1000\,\text{Å}$) of surface exposed to $0.027\,\text{L}\ O_2$ at 465 K after the region reached its asymptotic limit for structural evolution. Coalescence events occurred but could not fully extend due to oxygen depravation. (b) Relative population of single and double steps showing small changes for a dilute oxygen concentration.

for these conditions. There are many shorter coalescence events compared to the merges that are capable of happening (>1000 Å) if the system is given enough oxygen.

What we have determined is that the rate of doubling is extremely sensitive to the oxygen exposure to the surface. All of the coverage dependent experiments were performed at ~465 K where the step doubling process should not be limited by step edge mobility, i.e., the surface will double rapidly if supplied with enough oxygen. Why do we see variations in the rate constants for doubling at different coverages? We could only pose this question after witnessing how the merging proceeds in the STM. When one step edge reaches out across the terrace in the downstairs direction ([21 1]), makes contact with the adjacent edge, and there is sufficient oxygen, a step merge begins and continues to proceed for presumably as long as the oxygen concentration at the step edges is within a certain limit. If the doubling process is kinetically limited such that it will not occur unless the steps are mobile, then by running the coverage dependent experiments at high temperatures, the oxygen concentration should be the only factor influencing the merging. In the HAS study, the same experiment was performed where the doubling was studied as a function of oxygen coverage at one temperature. The macroscopic rate constants as well as the initial doubling rates were faster for more oxygen delivered to the surface. Why is it not the case that at the high temperature end of the doubling dynamic range, the initial rate of doubling would actually be the same regardless of coverage and only the extent to which the surface changes track with increasing oxygen? First we consider whether the diffusion of oxygen atoms on the surface at these doubling temperatures plays a role. Recent high speed STM measurements by Wintterlin *et al.* and Renisch *et al.* on O/Ru(0001) yield an oxygen hopping rate between sites at room temperature to be $16.6\pm0.9\,\text{s}^{-1}$ in the limit of dilute oxygen coverage and minimal interadsorbate interactions.[52,53] This corre-

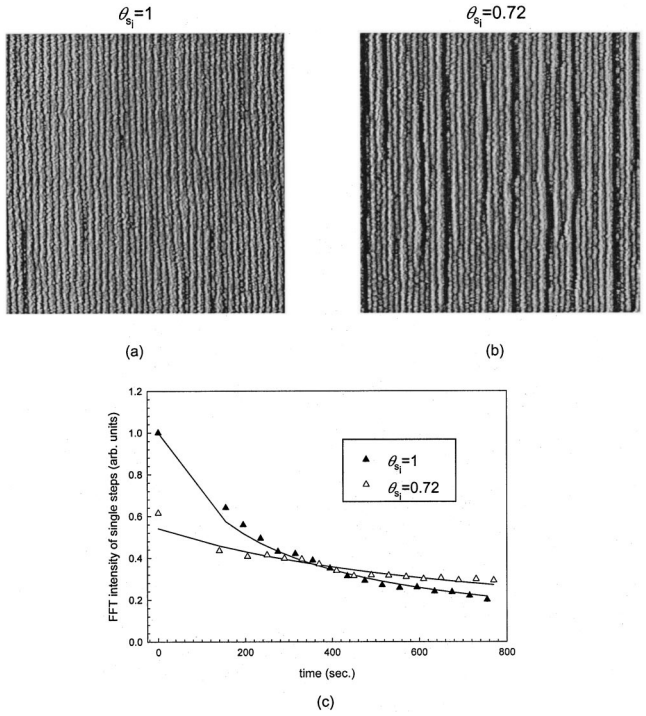

FIG. 10. (a) Region of single steps at 460 K. (b) Region of mixed single and double steps at 440 K. (c) FFT tracking of single step population for regions shown in (a) (filled triangles) and (b) (open triangles). The initial step density, which is a function of the initial single step population, θ_{S_i}, and therefore the number of step sites available for oxygen to adsorb to, is capable of influencing the rate of doubling. Doubling and singling for the two regions and two different single step populations, θ_{S_i}, shown in Fig. 10 after being exposed to 0.15 LO_2. Second order fits are plotted for the rate of single step population depletion. The rate of doubling and consequently the rate of single step intensity drop, are faster for the region that started with more single steps. The difference in the sample temperatures for the two different runs does not account for the slower rate.

sponds to a diffusion barrier of 0.55–0.7 eV. The hopping rate should increase exponentially with temperature but will be reduced by the interactions between oxygen adatoms. For O/Ni(100), Kopatzki and Behm cited a hopping frequency of $3\times10^{-4}\,s^{-1}$ at room temperature with 0.16 ML coverage using STM.[54] We can estimate the rate of oxygen jumps for our elevated temperature experiments,

$$f = v\exp\left(\frac{-E_d}{k_bT}\right), \tag{5}$$

where f is the hopping frequency, v is the surface normal vibration frequency for O bonded to Ni(100) ($\sim10^{13}\,s^{-1}$), E_D is the barrier to diffusion or activation energy, and $k_b = 8.617\times10^{-5}$ eV/K. For chemisorbed species like O on Ni, the activation energy for diffusion is close to ~1 eV (20% of chemisorption bond energy ~5 eV) which yields a hopping rate in the dilute and higher coverage oxygen concentration limits of $2.34\times10^{5}\,s^{-1}$ and 216 s^{-1}, respectively, at 465 K. This obviously cannot be the limiting factor for why steps in the dilute oxygen coverage limit exhibit slower merging rates. The ability of oxygen atoms to diffuse, however, will be affected not only by the oxygen concentration but also by the possibility of dissolution of oxygen that might wander onto the terrace. A separate study performed by our group

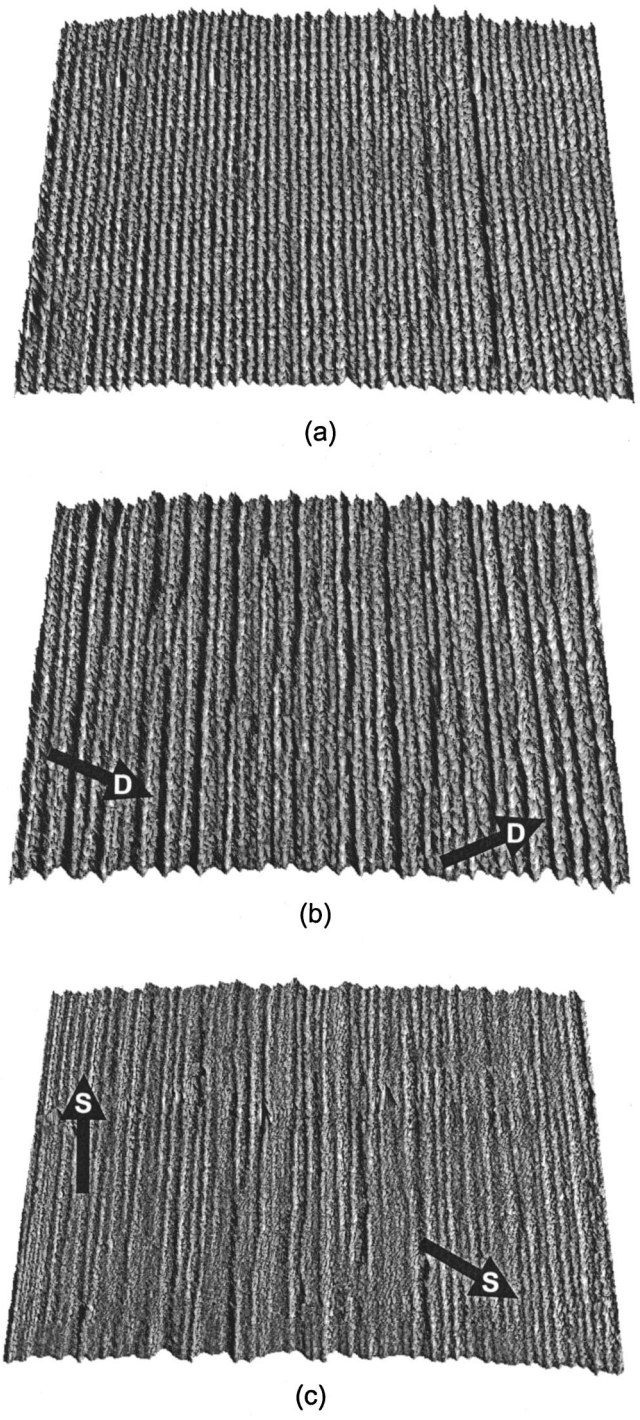

FIG. 11. Structural evolution of one region (1000 Å×1000 Å) at 465 K as a function of oxygen exposure. (a) Clean single steps. (b) Double steps formed by dosing 0.15 LO_2. (c) Return of single steps by dosing 0.3 L additional oxygen. The arrows indicate double and single steps that formed in (b) and (c), respectively.

suggests that while oxygen is stabilized at step edges, it is capable of dissolving through the terraces at temperatures as low as 440 K.[55] Some of the other results related to the dissolution issue will be discussed in more detail with the singling transition of the surface. We can conclude that the doubling process involves a concerted event that requires a critical number of oxygen atoms to be localized along both step edges that will potentially coalesce. From considering

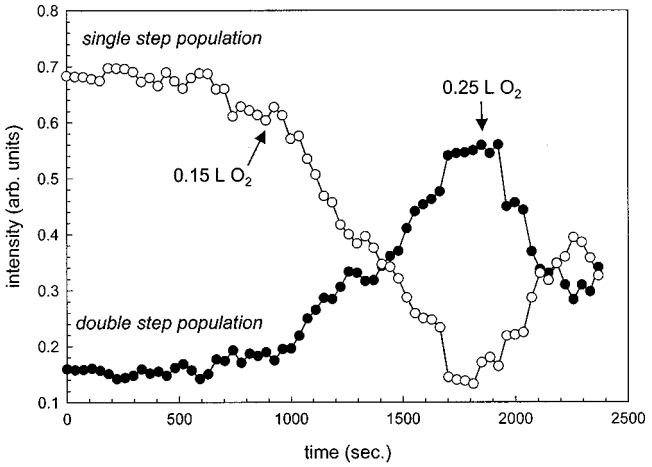

FIG. 12. Relative population of single and double steps as a function of time and oxygen dose at 465 K. Timing and magnitude of doses are indicated on the plot. The initial dose of 0.15 LO_2 doubles the surface while the exposure of the doubled surface to 0.25 LO_2 reverses the reconstruction. There is a clear inversion of populations for the two configurations as oxygen is sequentially dosed to the surface at temperature.

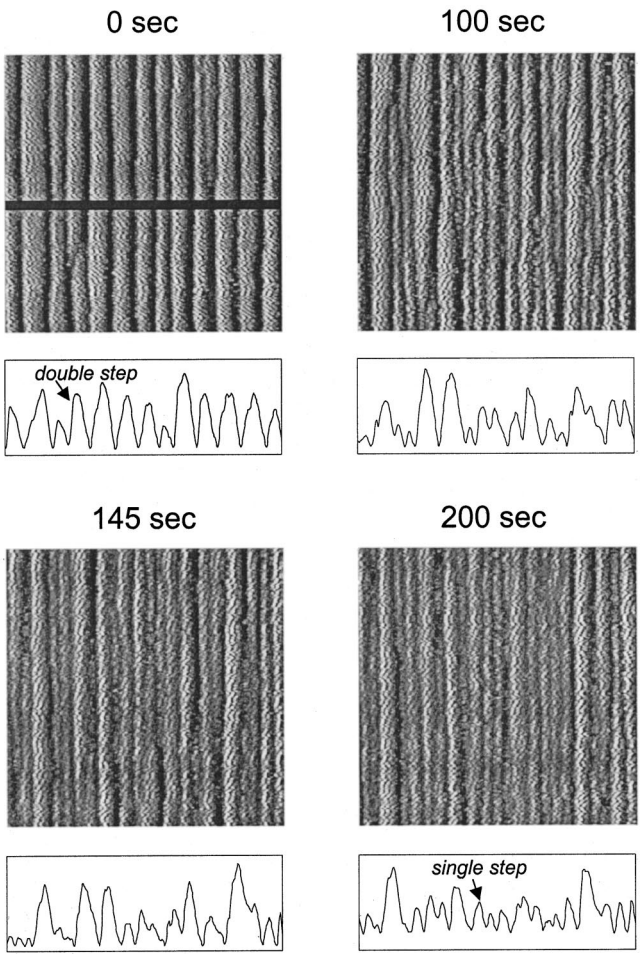

FIG. 13. 400 Å×400 Å regions at 465 K showing the rapid reversion of double steps back into single steps. The height profiles are clear indicators of the transition that has occurred between the four panels.

the coalescence in the low coverage regime [Fig. 9(a)] the shortest zippering event is approximately 100 Å which is a chain of about 20 oxygen atoms, with one at every other step site. Step doubling at lower coverages occurs in a more monotonic fashion due to the need for a critical build up of oxygen at two adjacent steps as shown by the gradual, relatively slow, evolution illustrated in Fig. 9.

This effect can also be seen at supersaturation of the step edges. By choosing to monitor an array of steps with a highly mixed concentration of step widths, we were able to capture the effect of having more than just step edge oxygen coverage. The assumption we made is that the oxygen will preferentially bind to all of the available single step edges and then attempt to populate other sites after the step edge sites are full. Two different regions are displayed in Fig. 10. The same amount of oxygen was then added to both areas (0.15 L) and then both doubling sequences were run at the high end of the temperature range for doubling (440 and 460 K). Figure 10(c) shows the difference in doubling rate for the two regions where the rate of doubling is faster for the region that started with more single steps. The ratio of the rate constants for the drop in singling population for these two areas is 3.7. This is a much larger than the 1.8 ratio found in the microscopic kinetics experiments (Fig. 7) where the step arrays started with far fewer nonsingle steps.

C. Resingling of surface

This vicinal surface can be driven by heat and a small amount of oxygen from single to double steps and then back to single steps with additional oxygen (Fig. 2). Figure 11 shows STM images of one region undergoing the structural phase transitions. The original reasoning for why the surface would revert to its original step configuration was that the ordered structures that grow out onto the terraces are energetically more favorable if they exist on single steps thereby making the double steps a relatively high free energy configuration. This defecating of the surface has been observed on both our sample and the Rh(332) system.[11] Figure 12 illustrates the evolution of single and double steps from FFT analysis where a very well reconstructed region can be driven back by unzippering to single step widths and heights. The resingling process was observed to occur rapidly with respect to doubling in localized areas presumably where either oxygen overlayers emanating from the step edge destabilize the double step structure or a critical subsurface concentration of oxygen had been reached (Fig. 13). While every stepped system with respect to crystallography and element will exhibit different behavior, there are some universal trends. The resingling of the surface, however, is not one of those processes. One possible scenario is that this conversion of double steps to single steps due to increased exposure of the surface to oxygen is the result of dissolution of oxygen into the double step terraces. Two observations lead us to believe this is viable. (1) Only vicinal systems composed of elements prone to oxygen dissolution to the subsurface or the bulk exhibit this behavior. Elements with much lower sticking coefficients for oxygen and a resistance to forming oxide or subsurface phases such as Pt and Cu have not been shown to undergo the same defecating transitions as a function of oxygen exposure.[1–4,13] Nickel readily absorbs oxygen at elevated temperatures and rhodium has been shown to form

subsurface oxygen structures at relatively low temperatures ($<$400 K).[56] (2) In a related study, we have results from studying the behavior of oxygen covered terraces at elevated temperature indicating that an ordered overlayer does remain on the surface at temperatures well above 440 K. There is a strong overlap between the range temperatures where the steps on the surface are mobile and the temperature range where we observe the oxygen to begin to dissolve. Oxygen is stabilized at the step edges and does not leave the surface until much higher temperatures ($\sim$565 K) but oxygen on the terraces may be finding a lower energy pathway to incorporation into the nickel bulk.[55]

IV. CONCLUSIONS

Elevated temperature time-lapse STM has been used to probe the adsorbate induced reconstruction behavior of Ni(977). Various observations regarding the nature of step–step interactions were made accessible by resolving morphological transformations in real time. There are a variety of factors that contribute to the overall probability of two steps merging. By monitoring this structural phase transition using a local probe, atomic-level mechanistic details for the step doubling and resingling transitions have been uncovered. Steps commence coalescence at a point contact or step edge bulge from one step to its downstairs neighbor step edge; doubling then proceeds via zippering. This long-standing question of the mechanism for the initiation and propagation of step coalescence in adsorbate driven surface reconstructions has been unambiguously answered through these measurements. Our observations enable us to argue that the local morphology plays a crucial role in determining whether two steps will actually merge by defining the number of step sites available for oxygen adsorption. Stability of the surface was likewise found to be strongly influenced by oxygen exposure where step arrangements were affected by the degree of step saturation of oxygen, as well as the level of oxygen dissolved in the selvedge region of the crystal. These observations provide insight into how the reaction pathways for a process like metallic oxidation are influenced by periodic defect structures. Details regarding atomic kink structure along the step edges, exact positioning of adatoms on the steps, and adsorbate influences on step mobility probability as well as the nature of the mobile species would further enhance the understanding of this phenomenon.

ACKNOWLEDGMENTS

The authors wish to thank Seth Darling and Aubrey Hanbicki for many enlightening discussions. This research was supported by the Air Force Office Scientific Research, with further support from the NSF-Materials Research Science and Engineering Center at the University of Chicago, Grant No. DMR-9808595.

[1] G. Comsa, G. Mechtersheimer, and B. Poelsema, Surf. Sci. **119**, 159 (1982).
[2] E. Hahn, A. Fricke, H. Röder, and K. Kern, Surf. Sci. **297**, 19 (1993).
[3] E. Hahn, H. Schief, V. Marsico, A. Fricke, and K. Kern, Phys. Rev. Lett. **72**, 3378 (1994).
[4] B. Lang, R. W. Joyner, and G. A. Somorjai, Surf. Sci. **30**, 454 (1972).
[5] A.-M. Lanzillotto and S. L. Bernasek, J. Chem. Phys. **84**, 3553 (1986).
[6] J. P. Chang and J. M. Blakely, J. Vac. Sci. Technol. A **10**, 2154 (1992).
[7] O. Haase, R. Koch, M. Borbonus, and K. H. Rieder, Phys. Rev. Lett. **66**, 1725 (1991).
[8] R. Koch, O. Haase, M. Borbonus, and K. H. Rieder, Surf. Sci. **272**, 17 (1992).
[9] H. E. Dorsett, E. P. Go, J. E. Reutt-Robey, and N. C. Bartelt, Surf. Sci. **342**, 261 (1995).
[10] D. G. Castner and G. A. Somorjai, Surf. Sci. **83**, 60 (1979).
[11] G. Hoogers and D. A. King, Surf. Sci. **286**, 306 (1993).
[12] M. Giesen, U. Linke, and H. Ibach, Surf. Sci. **389**, 264 (1997).
[13] G. Witte, J. Braun, D. Nowack, L. Bartels, B. Neu, and G. Meyer, Phys. Rev. B **58**, 13224 (1998).
[14] J. D. Batteas, J. C. Dunphy, G. A. Somorjai, and M. Salmeron, Phys. Rev. Lett. **77**, 534 (1996).
[15] J. C. Dunphy, C. Knight, P. Sautet, D. F. Ogletree, G. A. Somorjai, and M. B. Salmeron, Surf. Sci. **280**, 313 (1993).
[16] P. J. Knight, S. M. Driver, and D. P. Woodruff, Chem. Phys. Lett. **259**, 503 (1996).
[17] M. Giesen, Surf. Sci. **370**, 55 (1997).
[18] S. Goapper, L. Barbier, and B. Salanon, Surf. Sci. **409**, 81 (1998).
[19] L. Masson, L. Barbier, J. Cousty, and B. Salanon, Surf. Sci. **338**, 60 (1995).
[20] D. A. Walko and I. K. Robinson, Phys. Rev. B **59**, 15446 (1999).
[21] P. J. Knight, S. M. Driver, and D. P. Woodruff, Surf. Sci. **376**, 374 (1997).
[22] S. Kiriukhin, L. Sutcu, and E. H. Conrad, Phys. Rev. B **59**, 6736 (1996).
[23] S. Dey, S. Kiriukhin, J. West, and E. H. Conrad, Phys. Rev. Lett. **77**, 530 (1996).
[24] H. V. Thapliyal and J. M. Blakely, J. Vac. Sci. Technol. **15**, 600 (1978).
[25] J. S. Ozcomert, W. W. Pai, N. C. Bartelt, and J. E. Reutt-Robey, Phys. Rev. Lett. **72**, 258 (1994).
[26] J. T. Li, R. Berndt, R. Gaisch, and W.-D. Schneider, J. Vac. Sci. Technol. B **14**, 1149 (1996).
[27] S. Rousset, F. Pourmir, S. Gauthier, E. Lacaze, M. Sotto, J. Klein, and J. Lecoeur, J. Vac. Sci. Technol. B **14**, 1131 (1996).
[28] T. L. Einstein, T. M. Jung, N. C. Bartelt, and E. D. Williams, J. Vac. Sci. Technol. A **10**, 2600 (1992).
[29] T. M. Jung, R. J. Phaneuf, and E. D. Williams, Surf. Sci. **254**, 235 (1991).
[30] L. Niu, D. D. Koleske, D. J. Gaspar, S. F. King, and S. J. Sibener, Surf. Sci. **356**, 144 (1996).
[31] E. D. Williams and N. C. Bartelt, Science **251**, 393 (1991).
[32] C. Herring, Phys. Rev. **82**, 87 (1951).
[33] R. Smoluchowski, Phys. Rev. **60**, 661 (1941).
[34] C. Jayaprakash, C. Rottman, and W. F. Saam, Phys. Rev. B **30**, 6549 (1984).
[35] E. D. Williams, Surf. Sci. **299/300**, 502 (1994).
[36] M. M. Kamna, S. J. Stranick, and P. S. Weiss, Science **274**, 118 (1996).
[37] M. M. Kamna, T. M. Graham, J. C. Love, and P. S. Weiss, Surf. Sci. **419**, 12 (1998).
[38] X. Chen, E. R. Frank, and R. J. Hamers, J. Vac. Sci. Technol. B **14**, 1136 (1996).
[39] J. H. Ferris, J. G. Kushmerick, J. A. Johnson, and P. S. Weiss, Surf. Sci. **446**, 112 (2000).
[40] L. Niu, D. J. Gaspar, and S. J. Sibener, Science **268**, 847 (1995).
[41] D. J. Gaspar, A. T. Hanbicki, and S. J. Sibener, J. Chem. Phys. **109**, 1 (1998).
[42] S. B. Darling, A. T. Hanbicki, T. P. Pearl, and S. J. Sibener, J. Phys. Chem. B **103**, 9805 (1999).
[43] A. T. Hanbicki, S. B. Darling, D. J. Gaspar, and S. J. Sibener, J. Chem. Phys. **111**, 9053 (1999).
[44] S. V. Khare, T. L. Einstein, and N. C. Bartelt, Surf. Sci. **339**, 353 (1995).
[45] G. Witte and J. P. Toennies, Phys. Rev. B **55**, 1395 (1997).
[46] A. Kara, S. Durukanoglu, and T. S. Rahman, J. Chem. Phys. **106**, 2031 (1997).
[47] K. A. Thompson and C. S. Fadley, Surf. Sci. **146**, 281 (1984).
[48] T. P. Pearl and S. J. Sibener, Rev. Sci. Instrum. **71**, 124 (2000).
[49] L. Eierdal, F. Besenbacher, E. Laegsgaard, and I. Stensgaard, Surf. Sci. **312**, 31 (1994).
[50] T. P. Pearl and S. J. Sibener J. Phys. Chem. B (in press).
[51] C.-L. Liu and J. B. Adams, Surf. Sci. **265**, 262 (1992).

[52] S. Resnich, R. Schuster, J. Wintterlin, and G. Ertl, Phys. Rev. Lett. **82**, 3839 (1999).
[53] J. Wintterlin, J. Trost, S. Resnich, R. Schuster, T. Zambelli, and G. Ertl, Surf. Sci. **394**, 159 (1997).
[54] E. Kopatzki and R. J. Behm, Surf. Sci. **245**, 255 (1991).
[55] T. P. Pearl, S. B. Darling, and S. J. Sibener, Surf. Sci. (submitted).
[56] K. D. Gibson, M. Viste, E. Sanchez, and S. J. Sibener, J. Chem. Phys. **112**, 2470 (2000).